Viscoelastic Model for Redundancy Resolution of the Human Arm via the Swivel Angle: Applications for Upper Limb Exoskeleton Control

Hyunchul Kim, Jay Ryan Roldan, Zhi Li, and Jacob Rosen

Abstract— **One of the key research efforts associated with a redundant seven degree of freedom (7-DOF) upper limb exoskeleton robot that is mechanically coupled to the human body is to develop high and low level control algorithms that enable the system to become a natural extension of the human body. Improving the synergistic relationship between the exoskeleton and the operator is manifested in part by decreasing the force exchange between the two entities. Such a reduction is accomplished in part by developing criteria for resolving the human arm redundancy. The redundancy may be represented by a swivel angle which is defined as the angular rotation of the elbow around an axis that passes through the shoulder and wrist joints. The proposed criteria for defining the swivel angle takes into account the dynamics of the human arm along with a viscoelastic muscle-like model with variable damping. The swivel angle is estimated using the pseudo-inverse of the Jacobian with a secondary objective function that estimates the desired joint angles during human arm movement. The result is then fed to the muscle model to create a more realistic human motion. The estimated swivel angle is then compared with the actual swivel angle measured experimentally by a motion capture system. Results indicate that the average error between the estimated and measured swivel joint angle is 4.4 degrees (in the range [3.7-6] degrees), which are lower than the kinematically based redundant resolution criterion.**

I. Introduction

One of the key research efforts associated with a 7-DOF exoskeleton robot is to provide synchronized movements between operator and robot. As a result, one of the research directions in this framework is focused on the reduction of energy exchange between operator and robot based on deeper understanding of human arm motions. Liu et al. [1] proposed an advanced motion-planning scheme which provides proper joint configurations at key path points in the velocity level. Recent work in [2] showed that the arm posture at a particular target location is affected by both kinematics and dynamics, and their contribution depends on task complexity. Lussanet, et al. [3] presented a muscle model based on a mass-spring damper which creates the natural single-degree-of-freedom elbow joint movement. Due to lack of knowledge about the human motion planning mechanism, a control mechanism that provides seamless integration of the two systems is important. From our previous work [4], the swivel angle estimation algorithm only accounts for a purely kinematic aspect of the upper limb movement. Since the human arm is made up of muscle and bone structures that affects the dynamics arm motions, a control mechanism that includes arm velocity and acceleration in the swivel angle estimation creates a more human-like movement. In this paper we propose a control mechanism for a 7-DOF exoskeleton robot that can mimic natural human arm movement based on a biologically inspired constraint combined with a muscle model, which supports the dynamics of the human arm movement. Since grabbing and reaching tasks make up the majority of arm movements during daily activities, we focus on the control mechanism for natural reaching tasks, in this case without obstacles.

Hyunchul Kim Ph.D. is with the Dept. of Electrical Engineering, University of California Santa Cruz, Santa Cruz, CA
e-mail: hyunchul78@gmail.com
Jay Ryan Roldan BS, Zhi Li M.Sc., and Jacob Rosen Ph.D. are with the Dept. of Computer Engineering, University of California Santa Cruz, Santa Cruz, CA e-mails: juroldan@ucsc.edu , zhil@soe.ucsc.edu, rosen@ucsc.edu
Bionics Lab URL: http://bionics.soe.ucsc.edu/

II. Redundant Manipulator Inverse Kinematics

The position of the end effector $X = [x_1, x_2, \ldots, x_m]^T \in R^m$ in an n-link robot manipulator can be represented as $X = f(\theta)$ which is a function of joint space variables $\theta = [\theta_1, \theta_2, \ldots, \theta_n] \in R^n$. Note that f denotes the forward kinematic function. The reverse mapping of this is called the inverse kinematic. Once $X = f(\theta)$ is differentiated with respect to time, it can be rewritten as

$$\dot{X} = J\dot{\theta} \tag{1}$$

where J is the Jacobian that defines the relation between the task and joint space velocity as a function of θ. For a small time interval, J can be considered constant over the interval of the displacement and the general solution to Eq.1 can be approximated by

$$\dot{\theta} = J^{+}\dot{X} + \left(J^{+}J - I_n\right)z \tag{2}$$

where J^{+} is the pseudo-inverse matrix of J, I_n is the $n \times n$ identity matrix and z is an arbitrary matrix. $J^{+}X$ and $\left(J^{+}J - I_n\right)z$ is the minimum norm solution and homogeneous solution of Eq.1. For a redundant manipulator $(n > m)$, inverse kinematic solutions are not unique. Applying a proper cost function P to z as a secondary criterion defines a unique solution. By projecting P onto the null space of the Jacobian through $\left(J^{+}J - I_n\right)z$ Eq.2 can be written as

$$\dot{\theta} = J^{+}\dot{X} + \alpha_w \left(J^{+}J - I_n\right)\frac{\partial P(\theta, \theta_c(t))}{\partial \theta}, \alpha_w > 0 \tag{3}$$

where α_w is a weighting parameter. The following quadratic objective, called joint angle availability, was proposed by Liegeois [5] to allow the manipulator to avoid joint limits.

$$P(\theta, \theta_c(t)) = \sum_{i=1}^{n}\left(\frac{\theta_i - \theta_{ci}(t)}{\Delta\theta_i}\right)^2 \tag{4}$$
$$\theta_c(t) = [\theta_{c1}(t), \theta_{c2}(t), \ldots, \theta_{cn}(t)], \quad \theta(t) = [\theta_1, \theta_2, \ldots, \theta_n]$$

where θ_i, $\Delta\theta_i$ and $\theta_{ci}(t)$ are the joint angle, operating range and desired joint angle of joint i respectively. Note that the use of Eq.4 in Eq.3 enables the joint configuration of a redundant manipulator to remain close to $\theta_{ci}(t)$. Thus we can make the manipulator interact with the surrounding environment by applying different $\theta_c^j(t)$ as follows.

$$\theta_c(t) = \theta_c^j(t), \left(T_{j-1} < t \leq T_j\right) \tag{5}$$

where $\theta_c^j(t) = [\theta_{c1}^j(t), \theta_{c2}^j(t), \ldots, \theta_{cn}^j(t)]^T$. For simplicity, $\theta_c(t)$ can be a piecewise constant, time-varying function depending on the task property. However in general $\theta_c^j(t)$ is a function of time. This technique can be applied to wearable robots where natural arm motion is necessary for movement synchronization. Since unique

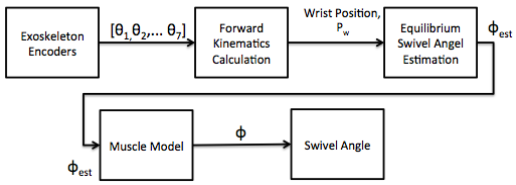

Fig. 1. A block diagram of the muscle model based swivel angle estimation.

human movement cannot be captured by the least norm solution in Eq.3, it is important to specify the desired joint configurations $\theta_c^j(t)$ for a natural arm posture as a basic control strategy for a complete control scheme.

III. Swivel Angle Estimation for Natural Arm Posture

The redundancy of the human arm represented as the swivel angle will be defined based on the 7-DOF arm model [6][7][8]. Once the swivel angle is resolved, the desired joint angles $\theta_c^j(t)$ can be defined. Fig. 1 shows the complete control scheme proposed in this paper.

In our previous work [4], it was shown that the swivel angle of the human arm for the unconstrained reaching task follows biological constraints. Given the role of the head as a cluster of sensing organs, it was hypothesized that the swivel angle is selected by the motor control system to efficiently retract the palm to the head region. In the following section, we briefly discuss the basic idea for the swivel angle estimation and describe the muscle model based on mass-spring with relative damping model.

A. Manipulability Ellipsoid and Optimum Swivel Angle

According to the above notion of efficient arm movement toward the head, the redundancy of the human arm can be closely associated with manipulability ellipsoid. Let P_m denote the virtual target position at the center of the head in Fig.2(a). When we consider the combinations of joint velocities satisfying the condition in which $\Sigma_{i=1}^{n}\dot{\theta}_i^{\,2}=1$, the hand velocity as a function of the joint velocity is described by an ellipsoid that defines the arm's scaled Jacobian [Fig.2(a)]. The largest among the major axes of the manipulability ellipsoid defines the best mapping between the joint space and the end effector (hand) space. It is therefore the direction in which the hand is more likely to move [9]-Fig.2(a). Assuming that virtual hand movement follows the shortest path connecting P_w to P_m, the swivel angle is chosen such that the projection of major axis of the manipulability ellipsoid onto (P_m-P_w) will be maximized.

Lemma 3.1: Given the inequality $\|P_w-P_s\|>\|P_w-P_e\|$, the longest axis of the manipulability ellipsoid is coplanar with plane S, defined by P_w, P_e and P_s, and its magnitude σ_1 is expressed as

$$\sigma_1 = \sqrt{\lambda_1}=\sqrt{\left(\left(L_{ws}^2+L_{we}^2\right)+\left(L_{ws}^2+L_{we}^2\right)c_1\right)/2} \quad (6)$$
$$c_1=\sqrt{1-c_2},\ c_2=4L_{we}^2L_{ws}^2\sin(\varphi)^2/\left(L_{ws}^2+L_{we}^2\right)^2$$

where $L_{ws}=\|P_w-P_s\|$ and $L_{we}=\|P_w-P_e\|$.

Proof: The proof can be found in [4]. ■

Then the optimum swivel angle is defined such that the projection of the longest axis u_1 on the vector P_m-P_w is maximized for the given wrist position.

$$\phi = \underset{\alpha,\beta\in[0\ \ \pi/2]}{\arg\max}\ [u_1^T(P_m-P_w)] \quad (7)$$
$$= \underset{\alpha,\beta\in[0\ \ \pi/2]}{\arg\max}\ [\|u_1\|\|P_m-P_w\|\cos(\alpha)\cos(\beta)] \quad (8)$$

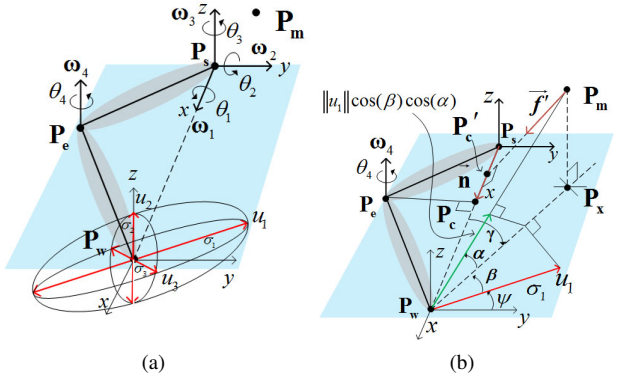

Fig. 2. Body coordinate system composed of points at the wrist (P_w), elbow (P_e) and shoulder (P_s), and a virtual point at the head region (P_m). In (b), γ is the angle between (P_s-P_w) and (P_x-P_w) while ψ is the angle between u_1 and (P_x-P_w).

where α and β are the angles between (P_m-P_w) and plane S, and the angle between u_1 and the projection of (P_m-P_w) onto S [Fig.2(b)] respectively. Note that the projected portion of u_1 onto (P_m-P_w) is represented by $\|u_1\|\cos(\alpha)\cos(\beta)$ and marked as a green arrow in Fig.2(b). Based on the geometry defined in Fig.2(b), $\cos(\alpha)\cos(\beta)$ is defined as

$$\cos(\alpha)\cos(\beta) = \frac{\|P_x-P_w\|}{\|P_m-P_w\|}\cdot\frac{c_3\|\vec{f}'\|\cos(\eta)+c_4\|P_c'-P_w\|}{\|P_x-P_w\|}$$
$$= \frac{c_3\|\vec{f}'\|\cos(\eta)+c_4\|P_c'-P_w\|}{\|P_m-P_w\|} \quad (9)$$
$$= c_5\cos(\eta)+c_6 \quad (10)$$

where c_3, c_4, c_5 and c_6 denote $\cos(\psi)$, $\sin(\psi)$, $c_3\|\vec{f}'\|/\|P_m-P_w\|$ and $c_4\|P_c'-P_w\|/\|P_m-P_w\|$ respectively. Then η in Eq.9 is the angle between $\vec{f}'$ and (P_c-P_e). The detailed proof for the equation can be found in [4]. Substituting the expression for $\cos(\alpha)\cos(\beta)$ in Eq.10 into Eq.8 results in

$$\phi = \underset{\alpha,\beta\in[0\ \ \pi/2]}{\arg\max}\ [\|u_1\|\|P_m-P_w\|(c_3\cos(\eta)+c_4)] \quad (11)$$

When $\eta=0$, Eq.11 is maximized and consequently $\alpha=0$ in Eq.8. Under this condition, plane S is coplanar with the plane defined by P_m, P_s and P_w. Then the swivel angle under this condition is calculated given the known positions P_m, P_w and P_s. In order to do so, a new vector $\vec{f}=P_w-P_m$ is defined. The vector $\vec{f}'$ is the projection of $\vec{f}$ on the direction of P_w-P_s in Fig.2(b). Based on the fact that $\vec{f}'$ is parallel to vector $P_e(\phi)-P_c$ when $\alpha=0$, the swivel angle is estimated by

$$\phi_{kin}=\arctan 2\left(\vec{n}\cdot\left(\vec{f}'\times\vec{u}\right),\vec{f}'\cdot\vec{u}\right) \quad (12)$$

B. Muscle Model based on Mass-Spring with Relative Damping Model

In general, estimating the motion of the arm involves the dynamics of the human arm which has certain stiffness and damping properties due to its muscle and bone structures. Thus by considering the dynamic property of the human arm in parallel with kinematic swivel angle estimation, more natural human arm movements can be created. In this context, a simple mass-spring with relative damping model was originally proposed to estimate a realistic arm movement such as a single degree of freedom elbow joint movement [3]. In

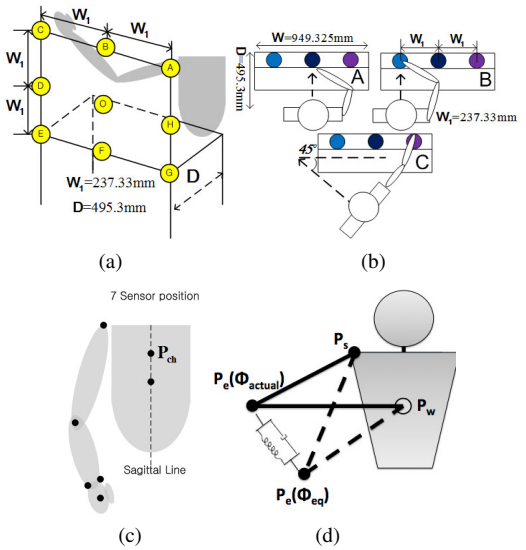

Fig. 3. a) Hand trajectory for data collection. b) Top view of three different tasks. c) Positions of LED markers: Shoulder (Acromioclavicular joint), Elbow (Lateral edge of the Ulna), Wrist (Medial & Lateral edge of the distal end of the radius & ulna), Palm(between 2 & 3 metacarples) and Torso (Upper & lower sternum) d) Mass-spring with relative damping model for the elbow movement of the human arm

this paper, damping and stiffness are defined between the desired and the actual elbow position with respect to the swivel angle as shown in Fig.3(d). According to this, the stiffness and damping effect exist along the circular trajectory of the elbow and all the muscles related to the elbow movements affect the dynamics of the human arm in aggregate. Eq.13 is the differential equation of a linear mass-spring system based on the relative damping model [3].

$$M\ddot{\phi} + B(\dot{\phi} - \dot{\phi}_{est}) + K(\phi - \phi_{est}) = 0 \tag{13}$$

where M, B and K are the mass, damping and stiffness respectively. Note that ϕ is the swivel angle and ϕ_{est} is the estimated equilibrium swivel angle for the given wrist position based on Eq.12; equivalently, $\phi_{est} = \phi_{kin}$. This relative damping model, considered as the damping with respect to the equilibrium point, makes the elbow tend to move at the same velocity toward the equilibrium elbow position $P_e(\phi_{est})$. In order to reduce the control parameter, Eq.13 is divided by M and rewritten as

$$\ddot{\phi} + b(\dot{\phi} - \dot{\phi}_{est}) + k(\phi - \phi_{est}) = 0 \tag{14}$$

where $b = B/M$ and $k = K/M$. For simplicity, it is assumed that an equilibrium swivel angle changes at a constant velocity and is piecewise linear for a small time duration.

$$\phi_{est}(t) = \phi_{est0} + \dot{\phi}_{est} \cdot t, \quad t \in [T_n, T_{n+1}], \tag{15}$$

where ϕ_{est0} is the initial velocity of each time duration. Note that the piecewise linear time duration $[T_n, T_{n+1}]$ is set to 0.1 sec for practical reasons. Then with boundary conditions $\phi(0) = \phi_0$ and $\dot{\phi}(0) = \dot{\phi}_0$, the solution for both the underdamped and overdamped case is shown below [3].

a) Underdamped Case $(k > b^2/4)$

$$\begin{aligned}\phi \quad = \quad & \dot{\phi}_{est} \cdot t + \phi_{est0} - \exp(-t/\tau)[(\phi_{est0} - \phi_0)\cos\omega t + \\ & \left(\frac{\dot{\phi}_{est} - \dot{\phi}_0}{\omega} + \frac{\phi_{est0} - \phi_0}{\omega\tau}\right)\sin\omega\tau],\end{aligned} \tag{16}$$

where $\tau = \frac{2}{b}$ and $\omega = \sqrt{k - \frac{1}{4}b^2}$.

b) Overdamped Case$(k < b^2/4)$

$$\begin{aligned}\phi = {} & \dot{\phi}_{est}t + \phi_{est0} - \frac{\tau_1}{(\tau_1 - \tau_2)}[(\dot{\phi}_{est} - \dot{\phi}_0)\tau_2 + \phi_{est0} - \phi_0] \\ & \exp(\frac{-t}{\tau_1}) + \frac{\tau_1}{(\tau_1 - \tau_2)}((\dot{\phi}_{est} - \dot{\phi}_0)\tau_1 + \phi_{est0} - \phi_0)\exp(\frac{-t}{\tau_2})\end{aligned} \tag{17}$$

where $1/\tau_1 = \frac{1}{2}b + \sqrt{\frac{1}{4}b^2 - k}$ and $1/\tau_2 = \frac{1}{2}b - \sqrt{\frac{1}{4}b^2 - k}$.

IV. Experiment and Results

There are three different experiments defined in Fig.3(b). For each experiment, subjects are seated in front of a task space with their torsional movement restricted as shown in Fig.3 and asked to naturally point to colored targets in a clockwise direction. In all cases, the joint locations are recorded by a motion capture system.

A. System and Protocol

The experimental setup is shown in Fig.3. The kinematic data of the human arm is collected using the Phasespace motion capture system (Phasespace, Inc.), which is equipped with eight cameras providing a millimeter accuracy at a distance of three meters. A 240Hz sampling rate is chosen to give excellent data density around potential occlusions that may occur. Active red LED makers are attached to each subject at key anatomical locations which includes the shoulder, elbow, wrist and chest [Fig.3]. Each subject is instructed to perform a reaching task described in Fig.3(b). The subjects place their hand at the center of the task space, target location O, and reach targets in sequence as follows, $A->B->C->D->E->F->G->H$ as shown in Fig.3(a). Reaching eight targets is one circuit. Each subject completes five circuits for each of the three different experimental conditions by moving their hand in a smooth path and stopping at each point using a self selected pace as illustrated in Fig.3(a). Reaching motions are performed without restrictions to hand orientation. The three experimental conditions are associated with the alignment of the torso in task space and designed to cover most of the right hand's work space. In condition (A) and (B), the torso is aligned with the center and the left blue circle respectively. The final condition (C) is with the torso turned forty five degree counterclockwise off the Sagittal alignment and the abducted hand points to the right purple circle. Five healthy subjects (three male and two female), aged from 20 to 38 participated in the experiment. Subjects were all right handed, the average height was 175.76cm.

B. Optimum P_m Estimation

Due to differences between subjects, it is important to optimally locate P_m for each subject. An LED marker P_{ch} located on the chest was used to estimate the location P_m. For this experiment it is assumed that the torso is restricted enough that the orientation is fixed, so P_m as a function of time is represented as

$$P_m(t) = P_{ch}(t) + P_o \tag{18}$$

where P_o is the fixed translation from P_{ch} with respect to the global frame. The optimal value of P_o is selected such that the difference between $\phi(t)_{est}$ – the estimated swivel angle based on Eq.12 and $\phi(t)_{act}$ – the calculated swivel angle based on the measured joint positions is minimized.

$$\underset{y,z \in U_s}{\arg\min} \int_y \int_z \left(\int_{t_x}^{t_x+T} |\phi(t)_{act} - \phi(t, P_o(y,z))_{kin}| dt \right) dz dy \tag{19}$$

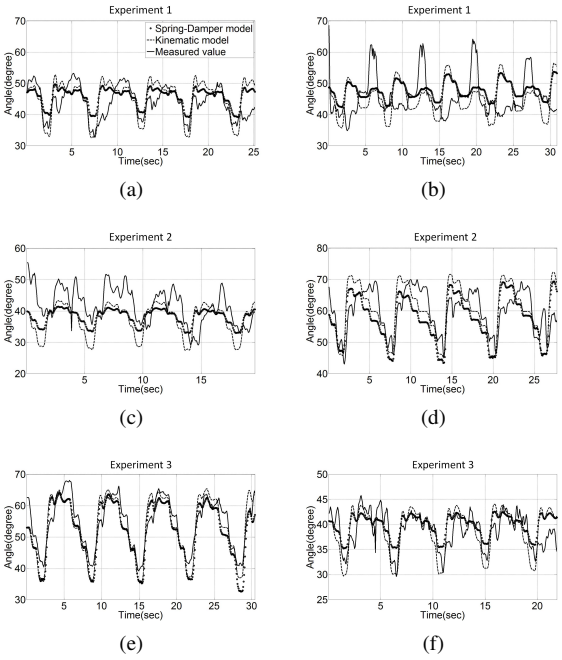

Fig. 4. Comparison between estimated swivel angle with muscle model (dotted), purely kinematic swivel angle (dashed) and measured swivel angle (solid) for two subjects. Each column corresponds to the result from one of the five subjects. Each row represents one of three different body orientation with respect to targets as shown in Fig.3(b).

where U_s is the (y,z) coordinate pair on the Sagittal plane equally dividing the human body in a vertical way. Since we assumed that P_m is located on the Sagittal plane, x_{opt} is the same as the x coordinate of $P_{ch}(t)$. For each data set only the first repetition of the entire data was used for fitting P_o. The actual P_o used for the subjects are summarized in Table I. Results show that estimated P_m with respect to the chest position is located on the face as we expected.

C. Optimum Parameter for the Muscle Model

Given the differences between subjects, it is important to estimate the optimum damping and stiffness parameter b and k for each subject. In order for this, matrix representation of Eq.14 is formulated as

$$\begin{bmatrix} -\ddot{\phi}(t_0) \\ -\ddot{\phi}(t_1) \\ \vdots \\ -\ddot{\phi}(t_{N-1}) \end{bmatrix} = \begin{bmatrix} a_1(t_0) & a_2(t_0) \\ a_1(t_1) & a_2(t_1) \\ \vdots & \vdots \\ a_1(t_{N-1}) & a_2(t_{N-1}) \end{bmatrix} \begin{bmatrix} b \\ k \end{bmatrix} \tag{20}$$

where $a_1(t) = \dot{\phi} - \dot{\phi}_{est}$ and $a_2(t) = \phi - \phi_{est}$. By replacing each term in Eq.20 with Y, A and X, the least square solution for Eq.20 is given by $X = (A^T A)^{-1} A^T Y$. Similarly from P_m estimation, only 20% of the entire data was used for fitting b and k for each subject; and these are summarized in Table.I.

D. Estimation Performance

Fig.4 shows the exemplary comparison results for three subjects and three types of experiments. We see that the swivel angle estimation based on the proposed muscle model estimates the actual swivel angle from each subject. For more quantitative analysis, the mean of the absolute estimation errors are also computed for each subject and each experimental set up (Table I). In most cases except

TABLE I
ESTIMATION ERROR

Sub	$P_o(mm)$	Muscle model	Mean of Absolute Error			
	(x_{opt}, z_{opt})	(b,k)	Exp 1 ϕ_{kin} ϕ	Exp 2 ϕ_{kin} ϕ	Exp 3 ϕ_{kin} ϕ	Total ϕ
1	(-160,280)	(188,175)	3.6° 3.0°	4.6° 4.3°	4.8° 4.5°	3.9°
2	(-140,320)	(177,107)	3.7° 3.5°	6.2° 5.9°	3.3° 3.2°	4.2°
3	(-70,290)	(179,100)	5.7° 4.3°	6.0° 5.2°	3.6° 3.1°	4.2°
4	(-140,330)	(107,37)	4.8° 4.7°	3.3° 3.3°	3.4° 3.2°	3.7°
5	(-60,220)	(92,20)	4.9° 5.4°	5.7° 6.6°	6.3° 6.1°	6.0°

the result for experiments 2 and 3 of subject 5, the mean value of the absolute estimation error is less than five degrees, and the muscle model output gives a better estimation result than the swivel angle estimation based on the purely kinematic constraint. Considering the imperfect joint location estimates, and inherent measurement error of the motion capture system, the estimation error in Table I can be regarded as a precise estimation result.

V. CONCLUSION

In this paper, the control scheme for the 7-DOF exoskeleton robot supporting the natural human arm movement for a simple reaching task is studied. The proposed algorithm estimates the swivel angle represented as the redundancy of the human arm based on the kinematic constraint combined with a muscle model that reflects the dynamic aspect of the human arm. Furthermore, the estimation results using the muscle model yield a more accurate estimate of the swivel angle compared to the purely kinematic constraint estimation. Improvements in the estimation were small due to naturally slow-reaching motion velocity and acceleration. For future work, studies must be done involving varying velocity and acceleration during reaching tasks. Although this model does not consider the full dynamic model including moment of inertia, centrifugal/coriolis forces and gravity force, the proposed control method provides a good estimation result for the human arm movement with low computational complexity. The proposed method can be considered as the realtime solution for the redundant 7-DOF exoskeleton robot mechanically coupled to a human arm.

REFERENCES

[1] T.-C. Liang and J.-S. Liu, "An improved trajectory planner for redundant manipulators in constrained workspace," *Journal of Robotic Systems*, vol. 16, no. 6, pp. 339–351, 1999.

[2] M. A.Admiraal, M. J. Kusters, and S. C. Gielen, "Modeling kinematics and dynamics of human arm movements," *Motor Control*, vol. 8, no. 3, pp. 312–338, 2004.

[3] M. H. de Lussanet, J. B. Smeets, and E. Brenner, "Relative damping improves linear mass-spring models of goal-directed movements," *Human Movement Science*, pp. 85–100, 2002.

[4] H. Kim, L. Miller, and J. Rosen, "Redundancy resolution of a human arm for controlling a seven dof wearable robotic system," in *IEEE international conference on EMBC*, Boston, USA, August 30 September 3 2011.

[5] A. Liegeois, "supervisory control of the configuration and behavior of multibody mechanisms," *IEEE Trans Syst Man, Cybernetics SMC-7*, pp. 868–871, 1977.

[6] J. U. Korein, *A Geometric Investigation of Reach*. MIT Press, 1985.

[7] I. Iossifidis and A. Steinhage, "Controlling a redundant robot arm by means of a haptic sensor," in *ROBOTIK 2002, Leistungsstand - Anwendungen - Visionen*, 2002, pp. 269–274.

[8] J. Rosen and J. C. Perry, "Upper limb powered exoskeleton," *International Journal of Humanoid Robotics*, vol. 4, no. 3, pp. 529–548, 2007.

[9] A. A. Maciejewski, "Dealing wit the ill-conditioned equations of motion for articulated figures," *IEEE Computer Graphics and Applications*, pp. 63–71, 1990.